SEISMIC RESPONSE OF RENYITAN EARTH-FILL DAM

Meen-Wah Gui[1] and Hsien-Te Chiu[2]

ABSTRACT

Taiwan is located at one of the earthquake-active zones. In 1999, a devastating 921 Chi-Chi earthquake struck Taiwan and caused severe property losses and thousands of lives. Excessive ground deformation caused severe crack to the Shigang concrete dam and resulted the dam to completely losses its ability to retain water. As such, assessing the safety of the water dams on the island has been emphasized. This study assessed the behavior of Renyitan dam using the acceleration record of Chi-Chi earthquake obtained some 2 km away as its input acceleration. Dynamic analyses were performed using the dynamic program FLAC^{2D} and results were evaluated from the viewpoint of displacement, excess pore-water pressure, and acceleration generated in the dam. Numerical results obtained confirmed that the generated excess pore-water pressures during the Chi-Chi earthquake were insufficient to cause the dam to liquefy or fail and pin-pointed the most likely location in the dam where liquefaction would be initiated. Strength improvement to the dam could be carried out at this weak area.

Key words: Earth-fill dam, numerical analysis, dynamic response, excess pore-water pressure, displacement, acceleration.

1. INTRODUCTION

Reservoir and dam are important to our daily life and the island of Taiwan has more than 50 dams with height greater than 15 m. According to Taiwan Water Resources Agency, the common forms of dam on the island are concrete gravity dam, concrete arch dam and earth-fill dam, in which earth-fill dam occupied nearly 50% (33 numbers) of them. Most of these earth-fill dams were rolling type earth-fill dam with a clay core to prevent seepage of water stored at the upstream.

Because Taiwan is located in the Circum-Pacific Seismic Zone, earthquake poses a very big threat to the safety of the dams and the population living in the downstream areas. For example, at 01:47 a.m. September 21, 1999, a strong earthquake measured 7.3 on the Richter scale struck Nantou County and inflicted severe damages and casualty to most parts of the island with 2,321 death and more than 8,000 people injured. The estimated properties lost were ten billions US dollars. The earthquake focused beneath the city of Chi-Chi at a depth of about 7-10 kilometers and many nearby dams received the shock and the after-shocks. A nearby concrete arch dam (Shigang dam) suffered severe ground heaved and caused the dam to shear off and lost its water storing capability. In addition, some of the nearby tourism spots and another nearby Re-Ye Tan dam were also suffered from a certain degree of damaged. Shuishe dam and Toushe dam generated crack of about 100 m long because of uneven heave and subsidence. After this earthquake, engineers in Taiwan began to focus on the earthquake response of the dams in Taiwan.

It is highly essential to understand the earthquake response of earth-fill dams. Rizendiz *et al*. (1982) gathered information on the earthquake induced reservoir damages in the world, and put forth six types of destructible forms: (i) sliding of dam slope or foundation; (ii) dam cracked; (iii) severe dam settlement that reduces the height of the spillway; (iv) fault sheared off dam and led to leakage; (v) dam overflowed; and (vi) shell liquefied. Out of these destruction forms, the most common one was the sliding of dam slope or foundation, which had a probability to occur of about 60% and it mainly occurred to early day's earth-fill dam constructed by hydraulic fill or earth-fill dam constructed on weak foundation, which may liquefy during an earthquake. It was found that earthquake caused less destruction to rolling-type earth-fill dam. International Committee on Large Dams (ICOLD, 1979) investigated dams with height greater than 15 m, and found that 50% of the destroyed dams had height between 15 m to 20 m. They also found that arch and gravity dams were the safest and second safest dam, respectively. Earth dam constituted 58% of all forms of built dam and that 74% of failed dam was earth-fill dam. Hence, the evaluation of dam safety is very important.

This study aims to understand the seismic response of one of the earth-fill dams, Renyitan dam, during the shaking of an earthquake. The background of Renyitan dam is first given. Dynamic analysis was then carried out for this dam using the program FLAC. The acceleration input was obtained from the acceleration history recorded during the Chi-Chi earthquake by an accelerometer located some 2 km away from the dam. The dynamic behavior of the dam was evaluated in terms of dam displacement, excess pore-water pressure, and acceleration recorded in the body of the dam.

2. BACKGROUND

2.1 Renyitan Dam

Jiayi government started planning the Renyitan dam in 1979 because of rapid industrial development and fast population increase, which in turn rapidly increase the demand of water consumption. Prior to this, the livelihood of the local community and industry depended on the underground water and the already under-supplied Lantan dam, which was located some 2.1 km

Manuscript received February 25, 2009; revised August 16, 2009; accepted August 17, 2009.

[1] Associate Professor (corresponding author), Department of Civil Engineering, National Taipei University of Technology, Taipei 106, Taiwan, R.O.C (e-mail: mwgui@ntut.edu.tw).

[2] Associate Technical Specialist, Zhongliao Township Administration Office, Nantou County, Taiwan, ROC; formerly, Department of Civil Engineering, National Taipei University of Technology, Taipei 106, Taiwan, R.O.C.

away. Construction of Renyitan dam at the upstream of the Bazhang River began in 1980 and it was completed in 1987. It is an off-stream dam with a height of 29 m and a 9 m wide crest. The dam is 1,535 m long with a water-storage area of about 3.66 square kilometer; the total water-storage capacity is about 29.11 million cubic meters, of which the effective water-storage capacity is 27.31 million cubic meters. Figure 1 shows a simplified cross-sectional of Renyitan dam.

The dam was founded on the Pliocene to the Pleistocene Toukoshan formation and modern alluvium. The Toukoshan formation was exposed and is mainly made up of pale green to gray mud siltstone, sandstone and mudstone that formed the sedimentary rock of the environment on the brink of the sea. The soil stratums of the site were divided from the top into alluvium, silty sandstone (silty sand/clay), sandstone (silty sand) and mudstone (batholith), respectively, of various thicknesses.

2.2 Dynamic Analyses of Earth-Fill Dam

The effect of hydrodynamic forces, which developed on the upstream slope, during severe transient excitations on a dam have been investigated by Chopra and Gupta (1981) and Chopra and Hall (1982). They carried out analysis in the frequency domain using finite element dam models. However, their procedures were mainly applied to concrete gravity and arch dams only (Bougachaa and Tassoulas, 2006). Lately, dynamic analysis of the interaction of pore fluid flow and porous structure has been explored by Wang and Wang (2007) via the simulation of the seismic response of a reservoir-earth dam-foundation system. However, the procedure is sophisticated and is still in the stage of development.

The three commonly performed dynamic analyses of earth-fill dam in Taiwan are the pseudo-static analysis, shear beam analysis, and finite element analysis. Pseudo-static analysis is the easiest form of dynamic analysis and it is a widely used method in evaluating the safety of earth-fill dams against sliding during earthquakes in which the effects of a complex earthquake force on a potential slide mass is simulated by an equivalent static horizontal force determined as the product of a seismic coefficient and the weight of the potential sliding mass (Terzaghi, 1950) The shear beam analysis (Mononobe *et al*., 1936) simplifies the two-dimensional earth-fill dam problem into a one-dimensional problem where the dam is simulated by a series of horizontal sheets, which are linked together by linear-elastic shear springs and viscous damping devices; the analysis can also be used to evaluate the natural vibration period of the dam. Finite element method is often used in geotechnical engineering for solving complicated problems. It divides a continuous body into several elements and derives the stress-strain relationship of each element by the equation of motion. The stresses and strains are then distributed among each element by material constitutive law and its shape function. Therefore, the vibration of the continuous body transforms into the vibration of each element. The equation of motion of a dam (Steven, 1996) can be written as:

$$\boldsymbol{M}\ddot{\boldsymbol{u}} + (\boldsymbol{K} + i\omega\boldsymbol{C})\,\boldsymbol{u} = -\boldsymbol{M}\boldsymbol{I}\ddot{\boldsymbol{u}}_{\boldsymbol{b}}(t) \tag{1}$$

where $\boldsymbol{M}$ = the mass matrix; $\boldsymbol{K}$ = the stiffness matrix; $\boldsymbol{C}$ = the damping matrix; $\ddot{\boldsymbol{u}}$, $\boldsymbol{u}$ are the nodal point accelerative and displacement (relative to the base) vectors, respectively; $\boldsymbol{I}$ = the identity matrix; and $\ddot{\boldsymbol{u}}_{\boldsymbol{b}}(t)$ = the time history of base acceleration. The solution of the dynamic response can be carried out in frequency domain or time domain, and output presented in the form of maximum shear stress and shear stress of time history.

3. NUMERICAL MODELING

Numerical analysis has been suited for analyzing wave propagation in continuous nonlinear media with large deformations because the complicated boundary conditions and soil models involved could be reasonably accounted for via simple equations (Stevens and Krauthammer, 1991). The finite difference program used in this study was FLAC^{2D} (Fast Lagrangian Analysis of Continua), which is well suited for modeling nonlinear systems (Itasca Consulting Group, Inc., 2002). The program adapts the dynamic equations of motion to ensure a stable numerical scheme when the physical system being modeled is unstable (Itasca Consulting Group, Inc., 2002).

FLAC is a commonly used finite difference method mainly used in geotechnical and mining engineering. In the analysis, the program divides the geometry of the dam into small elements via several grid lines. The elements behave according to a prescribed

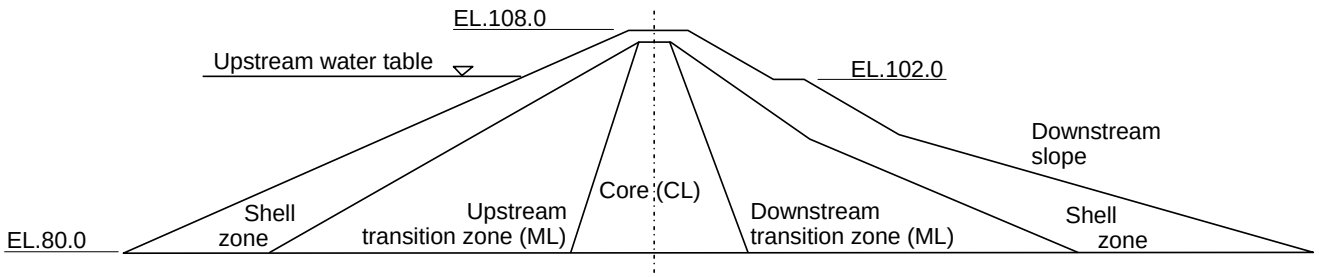

Fig. 1 Idealized cross-section of Renyitan dam

linear or non-linear stress/strain law in response to the applied forces or boundary restrains. The advantage of using FLAC for seismic analysis is the simplicity of applying seismic loading anywhere within the problem domain and the excellent post-processing capabilities (Itasca Consulting Group, Inc., 2002).

FLAC solved for every node the equations of motion in the time-stepping fashion. Thus, all calculation steps developed are related to time-step, but the time is not the real time it is merely the number of time-steps calculated. In every time-step, the unbalanced force that used in the original system determined the unbalance force of every node, and solved their equation of motion to derive new velocities. After deriving the new velocities, they will be integrated, so the displacements and increment of strains are solved subsequently. After the increment of strains was determined, increment of stresses was derived from the constitutive law of the material, and these added to the old stresses to become new stresses, and new unbalance forces derived. The calculation repeats itself until the unbalance forces are equal to zero, or close to zero.

3.1 Constitutive Model

Coupled dynamic-groundwater flow calculation can be performed with Finn model in FLAC^{2D}. Many researchers used it to analyze dynamic cases and the results were claimed to be closed to actual condition. For examples, Lee (2001) used it to simulate the earthquake-induced liquefaction of backfill behind caisson-type quay walls; and Hsu *et al*. (2003) used it to study the lateral spreading in Wufeng during the Chi-Chi earthquake.

The theory of Finn model is briefly given here. Detailed description of Finn model can be found in Martin *et al.* (1975). They analyzed many drained dynamic shear tests that were tested by Silver and Seed (1971) and discovered that the relation between the irrecoverable volume-strain relationship and cyclic shear-strain amplitude was independent of confining stress. They went further to supply the following relation between the decreased volumes of drained cyclic loading test and pore-water pressure rise of undrained test:

$$\frac{\Delta u \cdot n_p}{K_w} = \Delta\varepsilon_{vd} - \frac{\Delta u}{E_r} \tag{2}$$

where Δu = increment of pore-water pressure in each cycle, K_w = bulk modulus of water, n_p = porosity of soil, $\Delta\varepsilon_{vd}$ = decreased of volume-strain where sand structure slides, and E_r = reloading modulus = $(\sigma'_v)^{1-m} / mK_r(\sigma'_{vo})^{n-m}$, in which σ'_v = vertical effective stress, σ'_{vo} = original vertical effective stress, and m, n, K_r = experimental constants. Rearranging Eq. (2) to get

$$\Delta u = \frac{\Delta\varepsilon_{vd}}{\frac{1}{E_r} + \frac{n_p}{K_w}} \tag{3}$$

If the degree of saturation is 100%, the water can then be regarded as incompressible. With a large value of K_w, Eq. (3) can be simplified into

$$\Delta u = E_r \, \Delta\varepsilon_{vd} \tag{4}$$

Martin *et al.* (1975) used four constants to evaluate $\Delta\varepsilon_{vd}$:

$$\Delta\varepsilon_{vd} = c_1(\gamma - c_2 \, \varepsilon_{vd}) + \frac{c_3 \, \varepsilon_{vd}^2}{\gamma + c_4 \, \varepsilon_{vd}} \tag{5}$$

where γ = cyclic shear-strain amplitude, ε_{vd} = accumulated irrecoverable volume strain, and c_1, c_2, c_3, c_4 = constants. Martin *et al.* (1975) performed regression on tests data and derived that c_1 = 0.8, c_2 = 0.79, c_3 = 0.45, and c_4 = 0.73.

3.2 Materials Properties

In 1985, Taiwan Water Corporation appointed National Taiwan Institute of Technology (NTIT, 1987) to conduct tests for certain sections of the dam. The tests conducted were physical properties test, unsaturated unconsolidated undrained triaxial test, consolidated undrained triaxial test, and consolidated drained triaxial test. From the physical properties test results, the soil at the core was classified as low plasticity clayey soil (CL) and the soil at the transition zone was classified as low plasticity silty soil (ML). Consolidated triaxial tests were conducted for soil specimens obtained separately from the upstream transition zone, core, and downstream transition zone. The tests confining pressures varied between 100 and 400 kPa. The cohesion intercept c and friction angle ϕ obtained from the tests are shown in Table 1. The parameters for the shell region were suggested by Chang *et al*. (1996). The shell material has a cohesion intercept of 40 kPa because the intercept depended on whether a linear or a non-linear Mohr-Coulomb envelope was chosen to fit the laboratory data. If a non-linear envelope was fitted we would obtain a zero cohesion intercept, but if a linear envelope was fitted we would then expect a cohesion intercept. In this case, a linear envelope was obviously adopted.

4. SIMULATION OF RENYITAN DAM

4.1 Grid Generation

The first step of numerical analysis was to set up a numerical grid for the dam studied. Once the analysis started, the grid could not be changed until the end of the analysis. The dam was divided into five material zones: Upstream shell, upstream transition zone, core, downstream transition zone, and downstream shell (Fig. 1). Figure 2 shows the mesh of dam with 1056-elements.

4.2 Boundary Conditions

The bottom boundary of the dam was extended 10 m below the base of the dam (Fig. 2). The material at the foundation was clay, which was similar to the material of the core. The bottom boundary of the foundation was fixed in *x*- and *y*-directions. The left and right boundaries of the foundation soil were fixed in x-direction, and free in *y*-direction. Water pressure was specified along the water boundary on the upstream slope (slope surface directly beneath the water table).

Dynamic boundary is different from static boundary, and its function is to prevent the reflection of earthquake wave because when the waves reach free point, they will be reflected and affect the waves transmitted subsequently. Dynamic boundary can absorb the reflected earthquake wave. In FLAC^{2D}, dynamic boundary can be divided into quiet boundary and free-field boundary.

Table 1 Soil parameters adopted in the analysis

Parameters \ Zones	Shell zone	Upstream transition zone	Core zone	Downstream transition zone
Soil type	GM	ML	CL	ML
Dry unit weight, γ_d (kN/m^3)	20.0	17.2	18.1	17.9
Young's modulus, E (MPa)	50.0	39.79	60.31	24.53
Poisson's ratio, v	0.4	0.45	0.46	0.45
Cohesion intercept, c (kPa)	40	90	100	55
Friction angle, ϕ (^{o})	45	30	31	24
Coefficient of permeability (m/s) (Huang, 2003)	1×10^{-6}	1×10^{-7}	1×10^{-8}	1×10^{-7}

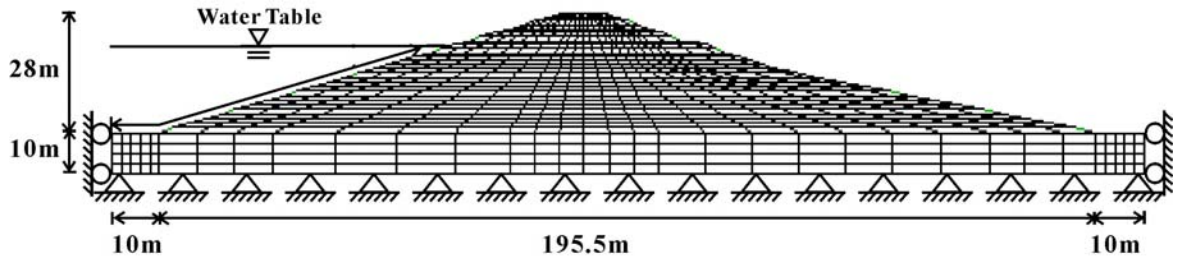

Fig. 2 Typical grid and boundary conditions used in FLAC (not to scale)

On one hand, quiet boundary is best suited when the dynamic source is within a grid but it should not be used along the side boundary of a grid when the dynamic source is applied as a boundary condition at the top or base, because the wave energy will "leak out" of the side (Itasca Consulting Group, Inc., 2002). On the other hand, if free-field boundary is applied to the side, plane waves propagating upward will not be distorted at the boundary because the free-field grid supplies conditions that are identical to those in an infinite model (Itasca Consulting Group, Inc., 2002). The type of dynamic boundary used in this study is free-field boundary.

4.3 Flow Analysis

Flow analysis was performed to obtain the initial pore-water pressure distribution in the dam. The full upstream water storage height of Renyitan dam is 24 m. The result of pseudo static analysis shown that as the water depth reduces, the factor of safety (*FOS*) also reduces until approximately half the water storage depth (12 m in this case) where a further reduction in water depth would instead increase the *FOS* of the dam (Gui and Wu, 2003). Therefore, water tables of 12 m and 24 m have been chosen to represent two extreme cases in the following dynamic analysis. The distribution of pore-water pressure is shown in Fig. 3. From the pore-water pressure contour, it can be seen that on a small fraction of water flowing through the lower left corner of the core. Most of the upper part of the core, the downstream transition zone and the downstream shell were in an unsaturated condition. The backward contour in the foundation region in Fig. 3(b) was caused by both the relatively high pore-water pressure and the relatively small coefficient of permeability of the CL soil. If water flows from a zone of a relatively high coefficient of permeability into a zone of a relatively low coefficient of permeability, we would observe a drop in the distribution of the pore-water pressure in this zone. The drop was seen in both the upstream transition zone and the core zone, where significant drop was seen in the least permeable core zone. The anticipated pore-water pressure distribution contour in the foundation region is shown in dotted lines in Fig. 3(b). Since we were interested in the excess pore-water pressure generated in the dam instead of its foundation, the backward contour in the foundation should not affect the interpolation of our result.

4.4 Acceleration History

In FLAC^{2D}, dynamic input can be provided using acceleration history, velocity history, stress (or pressure) history, or a force history. In addition, dynamic acceleration history can be determined using: (i) the accelerogram monitored during an earthquake, (ii) the artificially generated accelerograms, (iii) a modified accelerogram obtained from either (i) or (ii). This study used the first method to input the earthquake history. A

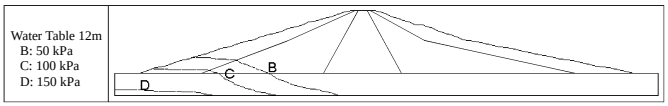

(a) 12 m upstream water tables

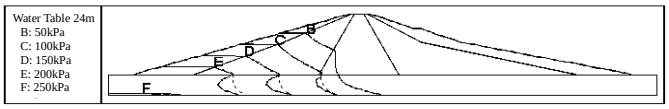

(b) 24 m upstream water tables

Fig. 3 Pore-water pressure contours

magnitude 5.5 earthquake was observed by a nearby accelerometer, located 2 km away from the dam. Figure 4 shows the input acceleration history.

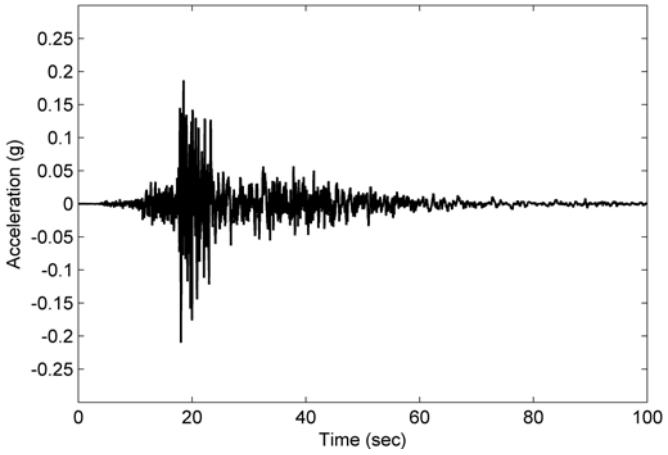

Fig. 4 Acceleration history used in the dynamic analysis

4.5 Rayleigh Damping

A dynamic numerical analysis must consider the energy loss or damping. Rayleigh damping is usually used in the analysis of structures and elastic continua to damp the natural oscillation modes of system. It is normally represented using a damping matrix $\boldsymbol{C}$ with components proportional to the mass $\boldsymbol{M}$ and stiffness $\boldsymbol{K}$ matrices (Itasca Consulting Group Inc., 2002):

$$\boldsymbol{C} = \alpha \boldsymbol{M} + \beta \boldsymbol{K} \tag{6}$$

where α = the mass-proportional damping constant, and β = the stiffness-proportional damping constant. For a multiple degree-of-freedom system, the critical damping ratio ξ_i at any angular frequency ω_i may be found using (Bathe and Wilson, 1976):

$$\alpha + \beta \omega_i^2 = 2\omega_i \, \xi_i \quad \text{or} \quad \xi_i = \frac{1}{2}\left(\frac{\alpha}{\omega_i} + \beta \omega_i \right) \tag{7}$$

By setting $\alpha = 0$ or $\beta = 0$, we obtain:

$$\alpha = \xi_{\min} \, \omega_{\min} \quad \text{and} \quad \beta = \frac{\xi_{\min}}{\omega_{\min}} \tag{8}$$

where $\omega_{\min}$ = the minimum angular frequency, and $\xi_{\min}$ = the minimum critical damping ratio. The minimum frequency is defined as:

$$f_{\min} = \frac{\omega_{\min}}{2\pi} \tag{9}$$

In FLAC, the damping parameters required are both the values of $f_{\min}$ and $\xi_{\min}$. For geological materials, the minimum critical damping ratio commonly falls in the range of 2% to 5% (Biggs, 1964); this study used 5%. For $f_{\min}$, if a wavelength for the fundamental mode of a particular system can not be estimated, then a preliminary run may be made with zero damping (Itasca Consulting Group Inc., 2002). A representative natural period may be estimated from time histories of velocity or displacement and $f_{\min}$ can be derived from the power spectrum (Itasca Consulting Group Inc., 2002). However, there are several definitions for power spectrum the one used in FLAC was adapted from Press *et al.* (1992), where the power spectrum is a set of $N/2$ real numbers defined as:

$$P_0 = \frac{1}{N^2} * \left(| \, f_0 \, | \right)^2 \quad \text{and} \quad P_k = \frac{1}{N^2} * \left[\left(| \, f_k \, | \right)^2 + \left(| \, f_{N-k} \, | \right)^2 \right] \tag{10}$$

where N = half the number of points in the original data field, P = the power spectrum output, f = the result of the Fast Fourier Transform of the original data, and k varies from 0 to $N/2$. Using this approach, $f_{\min}$ of 7.15 Hz has been found and used in all the subsequent analyses.

5. NUMERICAL RESULTS AND DISCUSSIONS

This section presents the results of the dynamic analysis of Renyitan dam. The dynamic response of the dam is presented in the forms of displacement, pore-water pressure, and acceleration.

5.1 Displacement

The results of the displacement generated during and after the earthquake shaking for 12 m and 24 m high upstream water tables are shown in Fig. 5. Figure 5(a) shows the location of the three settlement markers (VD1, VD2, and VD3) installed on the crest and the shoulder of the upstream and downstream slopes. Only the upstream slope displacement was influenced by the height of water table (Fig. 5(b)). For all locations, the maximum displacement was generated between t = 15 and 25 sec, coincided with the main earthquake strike. After the main strike, no further displacement was generated (Figs. 5(b) and 5(d)).

The displacement of the upstream slope for the case of 12 m high water table was greater than the displacement for the case of 24 m high of water table (Fig. 5(b)), whereas both the displacement profiles of the downstream slope were similar for both the 12 m and 24 m high water tables (Fig. 5(d)). This was because the hydrostatic water pressure, which was acting on the upstream slope, contributed as a restoring pressure and increased the stability of the upstream slope. Therefore, the maximum displacement recorded for the case of 24 m water table was only 2 cm compared to 3.2 cm in the case of 12 m water table. In other word, the upstream slope under 12 m of water table was more unstable than the case of 24 m of water table; this stability result was similar to the result obtained using the pseudo-static analysis (Gui and Wu, 2003). For the downstream slope a displacement of

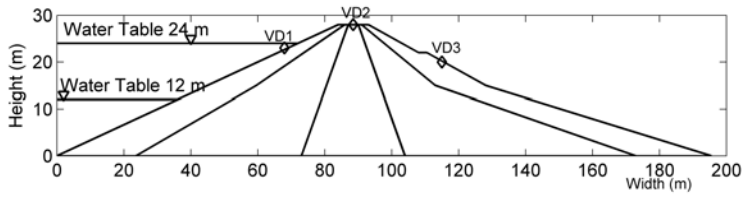

Width (m)
(a) Sectional drawing of Renyitan dam

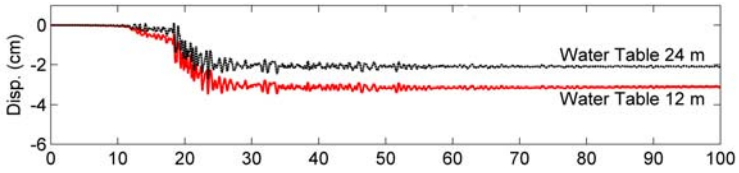

Time (sec)
(b) VD1 on upstream slope

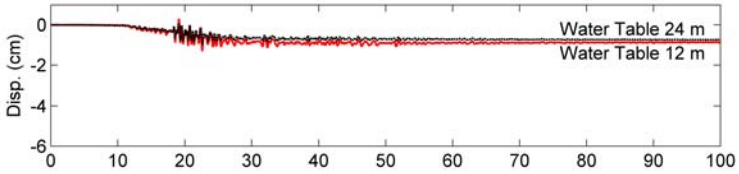

Time (sec)
(c) VD2 on dam crest

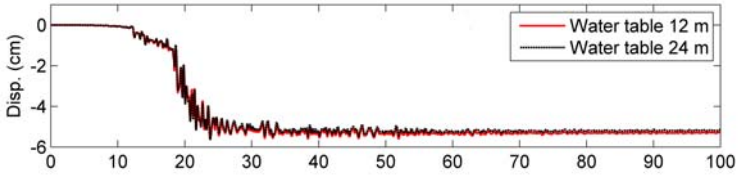

Time (sec)
(d) VD3 on downstream slope

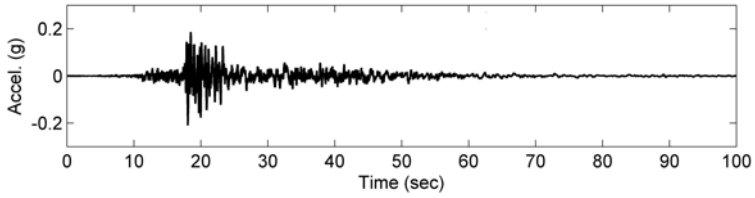

Time (sec)
(e) Input acceleration

Fig. 5 Displacement profiles

5.2 cm was observed for both the water tables, the condition was not affected by either the 12 or 24 m water tables as it was always dry, it thus produced the same displacement profile (Fig. 5(d)). Therefore, during an earthquake the upstream displacement profile would be different if the water table was different.

At the crest of the dam, the displacement obtained for the cases of 12 m and 24 m water tables was only about 8.7 mm and 7.3 mm, respectively (Fig. 5(c)). Thus, the height of the storage water table does not seem to have significant effect on the crest displacement. It is possible to verify the value of the above crest displacements with existing approximate method. For example, Bray and Travasarou (2007) proposed a simplified semi-empirical predictive relationship for estimating displacement due to earthquake-induced deviatoric deformations. Their recommended relationship for estimating the amount of nonzero seismic displacement, D, which is not biased due to magnitude, is

$$\ln(D) = -1.10 - 2.83\ln(k_y) - 0.333\left(\ln(k_y)\right)^2 + 0.566\ln(k_y)\ \ln\left(S_a(1.5T_s)\right) + 3.04\ln\left(S_a(1.5T_s)\right) - 0.244\left(\ln\left(S_a(1.5T_s)\right)\right)^2 + 1.50T_s + 0.278(M-7) \pm \varepsilon \quad (11)$$

where k_y = coefficient of yield acceleration, T_s = initial fundamental period of the sliding mass in seconds, $S_a(1.5T_s)$ = spectral acceleration of the input ground motion at a period of $1.5T_s$ in the units of g, ε = a normally distributed random variable with zero mean and standard deviation $\sigma = 0.66$, and M = magnitude. Bray and Travasarou (2007) also proposed the use of the following equation to estimate the initial fundamental period of the dam:

$$T_s = \frac{2.6H}{\hat{V}_s} \tag{12}$$

where $\hat{V}_s$ = average shear wave velocity. Typical value of $\hat{V}_s$ for fine sand to moist clay materials is about 164 m/s (Das, 1993) and with a dam height of 28 m, the initial fundamental period of Renyitan dam is thus 0.444 second. The coefficient of yield acceleration for a deep failure surface was estimated to be 0.25 and 0.20 for the cases of 12 m and 24 m water tables, respectively, from pseudo-static slope stability analyses performed with the strength properties as shown in Table 1. Note, however, that to obtain a deep failure surface the strength properties of the upstream shell zone has been assumed to be equal the strength properties of the upstream transition zone otherwise a shallow failure surface would be obtained. The spectral acceleration, $S_a(1.5T_s)$, of the input ground motion at a period of $1.5T_s = 0.67$ second, which was estimated from the acceleration response spectrum of the earthquake wave shown in Fig. 4, was 0.27 g. Using $M = 5.5$ and Eq. (11), displacements of 2.0 ~ 7.6 mm (median = 3.9 mm) and 3.6 ~ 13.4 mm (median = 6.9 mm) for the cases of 12 m and 24 m water tables, respectively, could be obtained. As mentioned earlier, the displacements obtained from the dynamic numerical analysis were 8.7 mm and 7.3 mm for the cases of 12 m and 24 m water tables, respectively, which was very close or fell within the range of the displacements predicted using the semi-empirical relationship of Bray and Travasarou (2007).

5.2 Pore-water Pressure

Excess pore-water pressure may be generated in sand during an earthquake shaking. If the excess pore-water pressure equals the effective stress of the soil, liquefaction occurs, and it leads to soil failure since soil can no longer sustain loading. This study used the ratio of excess pore-water pressure and initial effective stress within the dam to show the possibility of liquefaction occurring in the dam. Because results show that there was almost no or very little excess pore-water pressure generated near the surface of the dam, only the results of the pore-water pressure transducers (PPTs) installed near the bottom of the dam (Fig. 6(a)) are presented here. Figures 6(b) ~ 6(e) show the ratio of excess pore-water pressure generated and initial effective stress (U_{ex}) recorded in the upstream shell (PPT1), upstream transition zone (PPT2 and PPT3), and core zone (PPT4). It was interesting to note that the zone of maximum excess pore-water pressure was located near the base of the upstream transition zone (PPT2). This implied that if a dam was to liquefy during an earthquake, this would be the location for liquefaction or failure. This finding coincided with the result presented by Ming and Li (2003) whom employed a finite element program to analyze the San Fernando dam. Again, the maximum excess pore-water pressure was generated between t = 15 and 25 sec. As expected, the excess pore-water pressure generated under 24 m of water table was higher than the pore-water pressure generated under 12 m of water table (Figs. 6(b) ~ 6(e)). This was because to preserve the total stress, a soil element at some depth z with a small effective vertical stress must generate an excess pore-water pressure value that equals the difference between its total and effective vertical stresses. At locations of PPT1, PPT2, PPT3, and PPT4, their respective initial effective vertical stresses were higher in the case of 12 m water table than the 24 m water table. Therefore, to preserve the total stress at these locations, soil elements in the case of 24 m water table must generate a higher excess pore-water pressure than in the case of 12 m water table. The excess pore-water pressure generated quickly during the main earthquake, and is accumulated in such a way as described by the Finn model.

Severe fluctuation of excess pore-water pressure was seen in PPT1 (Fig. 6(b)). This was because PPT1 was in the gravelly shell zone of the dam, which has a much higher value of water coefficient of permeability; therefore, changes of pore-water pressure due to any fluctuation of water table during shaking could be instantaneously registered by this PPT. Figure 6(b) also shows that only some excess pore-water pressures were dissipated after the main shock, instead of fully dissipated, as we would have expected for material like gravel. This was mainly due to the Finn model used in the analysis, which tended to accumulate the pore-water pressure instead of "dissipating" it.

PPT2 and PPT3 were installed near the bottom of upstream transition zone. For PPT2, which was close to the shell zone, the excess pore-water pressure generated in both cases of the water table was about 60% of the initial effective stress (Fig. 6(c)). For PPT3, the excess pore-water pressure generated was about 52% and 40% of the initial effective stress, respectively, for 24 m and 12 m water tables (Fig. 6(d)). Therefore, the upstream shell was still a safe zone during the shaking as liquefaction was not lightly to occur under an acceleration of about 0.22 g.

In the core area (Fig. 6(e)), only negligible excess pore-water pressure–9% and 1% of the initial effective stress for 24 m and 12 m water table, respectively–was generated. This was because, for the case of 24 m water table, only a small fraction of water was flowing into the bottom-left corner of this almost impermeable zone (Fig. 3(b)) and almost no water was flowing into this almost impermeable zone for the case of 12 m water table (Fig. 3(a)). From the excess pore-water pressure ratio results, this should explain why the Renyitan dam was not liquefied or failed during the Chi-Chi earthquake.

Figures 7(a) and 7(b) show the most likely location for the largest pore-water pressure to generate during shaking. It can be seen that for both the 12 and 24 m water tables the most likely location in the dam for the largest pore-water pressure to generate was near the bottom-left corner of the upstream transition zone, implying that this would be the most likely location for liquefaction or failure to initiate.

5.3 Acceleration

During earthquake shaking, the influence of soil characteristics, soil thickness, and earthquake wavelength might magnify the earthquake acceleration (Okamoto, 1984). This is especially so for the trapezoidal shaped structure such as dam where the acceleration is magnified as it propagates from the base to the top of the dam. The question then became what was the magnification factor for the dam during the Chi-Chi earthquake? Magnification factor could be obtained by normalizing the maximum acceleration at any depth against the maximum acceleration at the base of the foundation or the input acceleration. The magnification factor at three depths of the core of the dam during the shaking under both the storage water tables was recorded and plotted in Fig. 8, where H = 28 m (EL. 108 m) corresponded to the crest of the dam. In general, the level of the storage water tables did not have any influences in the magnification factor of the core of the dam.

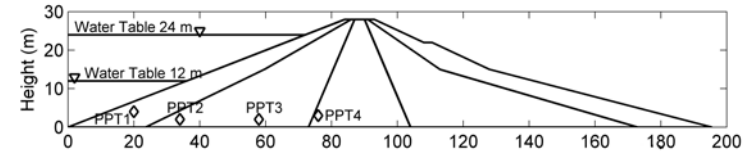

(a) Sectional drawing of Renyitan dam

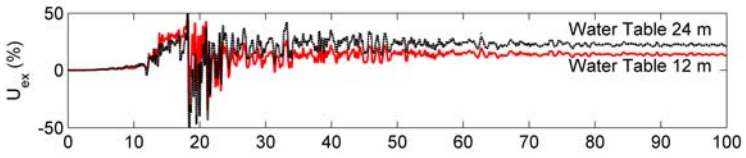

(b) at PPT1

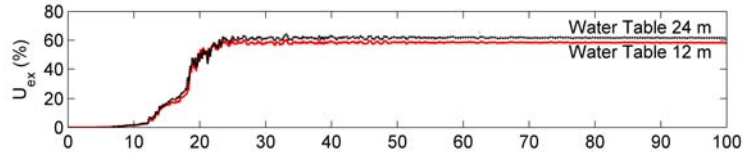

(c) at PPT2

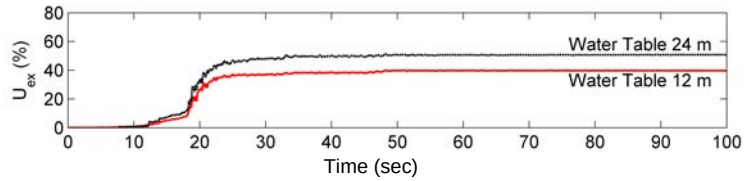

(d) at PPT3

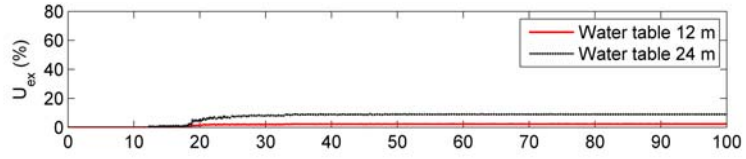

(e) at PPT4

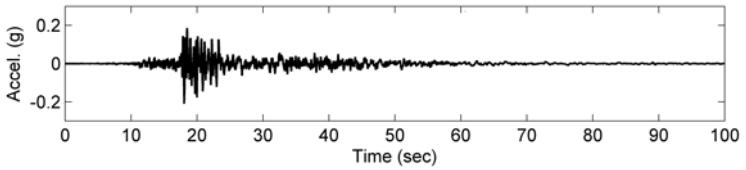

(f) Input acceleration

Fig. 6 Ratio of excess pore-water pressure and initial effective stress

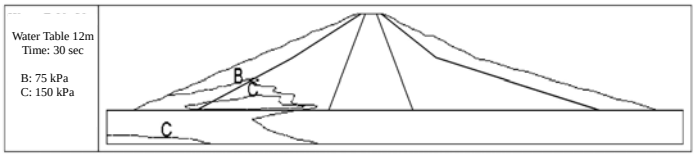

(a) 12 m water table

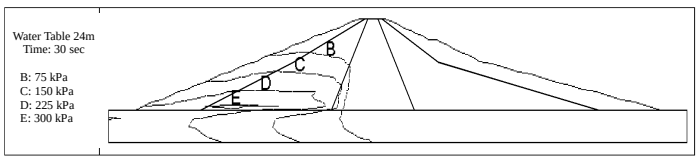

(b) 24 m water table

Fig. 7 Distribution of pore-water pressure at time *t* = 30 seconds

As earthquake travels from the base of the foundation to the crest of the dam, the magnification factor increases non-linearly. Magnification occurred as soon as propagation begins at the base of the foundation, probably because of the same material used for both the foundation and core areas. The maximum input acceleration was 0.22 g while the recorded maximum acceleration at the crest was 0.47 g, thus a maximum magnification factor of 2.13 was observed for the Renyitan dam during the Chi-Chi earthquake (Fig. 8). Seed *et al.* (1977), who analyzed many earth-fill dams behavior in the world, concluded that virtually any well- built dam on a firm foundation could withstand moderate earth- quake shaking with peak acceleration up to 0.2 g with no detrimental effects and that dams constructed on clay soils or rock foundations could withstand extremely strong shaking ranging

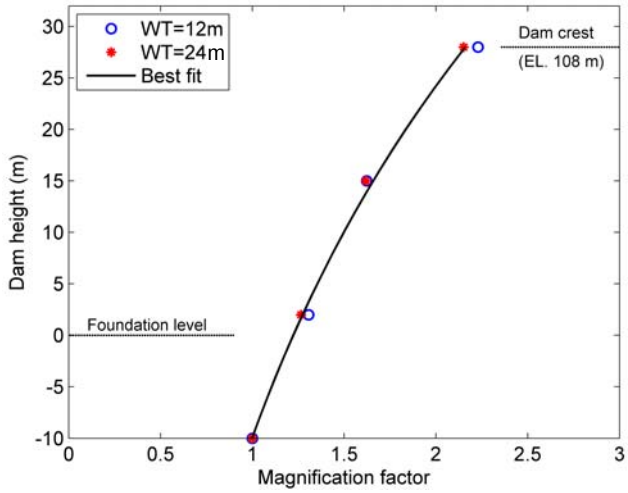

Fig. 8 Magnification factor obtained from three different depths of the core of the dam for both cases of storage water tables

from 0.35 to 0.8 g earthquake with no apparent damage. Since the numerically derived peak acceleration at the crest of the Renyitan dam was 0.50 g, which lies between the values suggested by Seed *et al.* (1977), no detrimental effect should be expected for this dam.

5.4 Limitation of Study

When an earth-fill dam is subjected to an earthquake, its behavior may be defined by the variation of deformation and pore-water pressure in the body of the dam itself. These readings could be measured on site via monitoring instrumentation or estimated via the numerical methods. However, landform, geology, dam geometry, in-situ materials, *etc*. are often difficult to quantify. The numerical results can only be used for qualitative judgment unless, of course, the results could be calibrated with field measured data first.

There were 42 numbers of pore-water pressure transducer installed at various locations of this dam but most of them were damaged due to lightning or worn down due to the lack of maintenance. No data from any of these pore pressure transducers was taken since September, 1998, *i.e.* one year before the Chi-Chi earthquake. In addition, 16 units of soil pressure gauges were also installed to measure soil stresses in the shell during the dam construction but because the readings were unreasonable, probably due to poor circuits contact, no measurements were ever taken after the dam construction.

Although the calibration of the above numerical results with field data was impossible, this study provided us a snapshot of the dynamic response of Renyitan dam during the Chi-Chi earthquake. To improve our knowledge in dynamic response of earth-fill dam, it is therefore imperative for monitoring instrumentation be installed, maintained and readings taken so that when earthquake occurred the vibratile response of the dam could be monitored and readings be used for the calibration of the subsequent numerical results.

6. CONCLUSIONS

A numerical study has been carried out to study the dynamic response and, hence, the stability of Renyitan dam during earthquake. The effects of two extreme cases (12 m and 24 m) of upstream storage water table on the displacement, excess pore- water pressure and acceleration distribution in this dam have been examined. During the earthquake shaking, a lower upstream water table would result in a larger upstream slope displacement and that the height of the upstream water table would not affect the downstream slope displacement profile. The largest excess pore-water pressure was found generated near the bottom-left corner of the upstream transition zone, implying that this would be the most likely location for liquefaction or failure to initiate. Because the core zone was almost unsaturated as not much water was flowing into this zone, only a small fraction of excess pore-water pressure was generated during shaking and, thus, liquefaction would be unlikely to occur in the core zone. Earthquake acceleration was magnified in a non-linear fashion as soon as it propagated upward from the base of the foundation to the crest of the dam.

ACKNOWLEDGEMENTS

The authors are grateful to the support provided by the National Science Council, Taiwan, under Grant No. NSC 91-2211-E-027-009.

REFERENCES

Bathe, K. J. and Wilson, E. L. (1976). *Numerical Methods in Finite Element Analysis*, Prentice-Hall, Inc., Eaglewood Cliffs, New Jersey.

Biggs, J. M. (1964). *Introduction to Structural Dynamics*, McGraw-Hill Book Co.

Bougacha, S. and Tassoulas, J. L. (2006). "Dam-water-sediment-rock systems: Seismic analysis." *Soil Dynamics and Earthquake Engineering*, **26**, 680–693

Bray, J. D. and Travasarou, T. (2007). "Simplified for estimating earthquake-induced deviatoric slope displacements." *Journal of Geotechnical and Geoenvironmental Engineering*, ASCE, **133**(4), 381–392.

Chang, C. T., Chen, Y. J., Yen, S. C. and Chai, Y. C. (1996). "Study of engineering properties and construction method for gravel formations in central and northern Taiwan." *Sino-Geotechnics*, **55**, 135–146 (in Chinese).

Chopra, A. K. and Gupta, S. (1981). "Hydrodynamic and foundation interaction effects in earthquake response of a concrete gravity dam." *Journal of the Structural Division*, ASCE, **107**(8), 1399–1412.

Chopra, A. K. and Hall, J. F. (1982). "Two-dimensional dynamic analysis of concrete gravity and embankment dams including hydrodynamic effects." *Earthquake Engineering and Structural Dynamics*, **10**, 305–332.

Das, B. M. (1993). *Principles of Soil Dynamics*. PWS-KENT Publishing Company, 570p.

Gui, M. W. and Wu, H. H. (2003). "Seismic analysis of Renyi dam in Taiwan." *Proc. 12th Asian Regional Conf. on Soil Mechanics and Geotechnical Engineering, Singapore*, 287–290.

Hsu, S. C., Chu, B. L. and Lin, C. C. (2003). "Study of lateral spreading in Wufeng during 921-Chi-Chi Earthquake." *Proc. 10th Taiwan Geotechnical Engineering Conference*, 893–896.

Huang, C. F. (2003). *Feasibility Study of Alert Monitoring System for Seismic Earthfill Dams*. Master Thesis, National Taipei University of Technology, Taiwan.

ICOLD (1979). *World Register of Dams, 2nd Updating*. International Commission on Large Dams, Paris.

Itasca Consulting Group, Inc., (2002). Fast Lagrangian Analysis of Continua user's guide, FLAC^{2D} version 4.0, Minneapolis, Minnesota, USA.

Lee, C. H. (2001). *Numerical Modeling of Earthquake-Induced Liquefaction of Backfill Behind Caisson Type Quay Walls*. Master Thesis, National Central University, Taiwan.

Martin, G. R., Finn, W. D. L. and Seed, H. B. (1975). "Fundamentals of liquefaction under cyclic loading." *Journal of Geotechnical Engineering Division*, ASCE, **101**(5), 423–438.

Ming, H. Y. and Li, X. S. (2003). "Fully coupled analysis of failure and remediation of lower San Fernando dam." *Journal of Geotechnical and Geoenvironmental Engineering*, ASCE, **129**(4), 336–349.

Mononobe, N., Takata, A. and Matumura, M. (1936). "Seismic stability of the earth dam." *Trans. 2nd Congress on Large Dams (CLD'36)*, Washington, D.C., 435–444.

National Taiwan Institute of Technology, NTIT (1987). *Soil Testing Report for Renyitan Dam Earth-filled Materials* (in Chinese).

Okamoto, S. (1984). *Introduction to Earthquake Engineering*. University of Tokyo Press, 2nd Ed., 630p.

Press, W. H., Flannery, B. P., Teukolsky, S. A. and Vetterling, W. T. (1992). *Numerical Recipes in C: The Art of Scientific Computing*. Cambridge University Press, Cambridge and New York, 2nd Ed.

Rizendiz, D., Romo, M. P. and Moreno, E. (1982). "E1 information and La Villita dams: seismic behavior." *Journal of Geotechnical Engineering Division*, ASCE, **108**(1), 109–131.

Seed, H. B., Makdisi, F. I. and de Alba, P. (1977). "The Performance of earth dams during earthquakes." *Report No.EERC-77/20, EERC*, University of California, Berkeley.

Silver, M. L. and Seed, H. B. (1971). "Volume changes in sands during cyclic loading." *Journal of the Soil Mechanics and Foundations Division*, ASCE, **97**(9), 1171–1182.

Steven, H. W. (1996). "Measurements of the complex moduli and damping of soils under dynamic loads." *US Army Cold Regions Research and Engineering Laboratory, Hanover, N.H., Technical Report, No 173*, **13**(3).

Stevens, D. J. and Krauthammer, T. (1991). "Analysis of blast-loaded, buried RC arch response. I: Numerical approach." *Journal of Structural Engineering*, ASCE, **117**(1), 197–212.

Terzaghi, K. (1950). *Mechanism of Landslides. Application of Geology to Engineering Practice (Berkey Volume)*, Edited by S. Paige, The Geological Survey of America, New York, 83–123.

Wang, X. and Wang, L. B. (2007). "Dynamic analysis of a water-soil-pore water coupling system." *Computers and Structures*, **85**, 1020–1031.